Noninvasive Evaluation of CD20 Expression Using ^{64}Cu-Labeled F(ab′)$_2$ Fragments of Obinutuzumab in Lymphoma

Lei Kang*[1,2], Cuicui Li*[1], Zachary T. Rosenkrans[3], Jonathan W. Engle[2], Rongfu Wang[1], Dawei Jiang[2,4], Xiaojie Xu[5], and Weibo Cai[2,3]

[1]Department of Nuclear Medicine, Peking University First Hospital, Beijing, China; [2]Departments of Radiology and Medical Physics, University of Wisconsin–Madison, Madison, Wisconsin; [3]Department of Pharmaceutical Sciences, University of Wisconsin–Madison, Madison, Wisconsin; [4]Department of Nuclear Medicine, Union Hospital, Tongji Medical College, Huazhong University of Science and Technology, Wuhan, China; and [5]Department of Medical Molecular Biology, Beijing Institute of Biotechnology, Beijing, China

CD20-overexpressed non-Hodgkin lymphoma typically indicates progressive malignancy. Obinutuzumab is a next-generation Food and Drug Administration–approved humanized monoclonal antibody that targets CD20. Previous studies with ^{89}Zr-labeled obinutuzumab have successfully imaged CD20 in vivo. However, delayed tumor uptake and increased radioactive exposure caused by long blood circulation limit its clinical translation. This study aimed to develop ^{64}Cu-labeled F(ab′)$_2$ fragments of obinutuzumab for imaging CD20 in lymphoma xenograft tumor models. **Methods:** F(ab′)$_2$ fragments were produced from obinutuzumab using an IgG-degrading enzyme of *Streptococcus pyogenes* (IdeS) enzyme and purified with protein A beads. Sodium dodecyl sulfate polyacrylamide gel electrophoresis and high-performance liquid chromatography were performed to evaluate the products and their stability. F(ab′)$_2$ products were conjugated with p-SCN-Bn-NOTA (NOTA) for ^{64}Cu radiolabeling. Western blotting was performed to screen the CD20 expression levels of lymphoma cells. Enzyme-linked immunosorbent assay, flow cytometry, and confocal imaging were used to test the binding affinity in vitro. Serial PET imaging and biodistribution studies in subcutaneous lymphoma–bearing mice were performed using ^{64}Cu-NOTA-F(ab′)$_2$-obinutuzumab or ^{64}Cu-NOTA-F(ab′)$_2$-IgG. **Results:** F(ab′)$_2$-obinutuzumab and F(ab′)$_2$-IgG produced by the IdeS digestion system were confirmed with sodium dodecyl sulfate polyacrylamide gel electrophoresis and high-performance liquid chromatography. The radiochemical purity of ^{64}Cu-labeled F(ab′)$_2$ fragments was no less than 98%, and the specific activity was 56.3 ± 7.9 MBq/mg (n = 6). Among the 5 lymphoma cell lines, Ramos showed the strongest expression of CD20, and CLL-155 showed the lowest, as confirmed by enzyme-linked immunosorbent assay, flow cytometry, and confocal imaging. PET imaging revealed rapid and sustained tumor uptake of ^{64}Cu-NOTA-F(ab′)$_2$-obinutuzumab in Ramos tumor–bearing mice. The peak tumor uptake (9.08 ± 1.67 percentage injected dose per gram of tissue [%ID/g]) in the Ramos model was significantly higher than that in the CCL-155 model (2.78 ± 0.62 %ID/g) or the ^{64}Cu-NOTA-F(ab′)$_2$-IgG control (1.93 ± 0.26 %ID/g, n = 4, $P < 0.001$). The tumor-to-blood and tumor-to-muscle ratios were 7.3 ± 1.6 and 21.9 ± 9.0, respectively, at 48 h after injection in the ^{64}Cu-NOTA-F(ab′)$_2$-obinutuzumab group. Of the measured off-target organs, the kidneys showed the highest uptake. Ex vivo immunofluorescent staining verified the differential CD20 expression in the Ramos and CCL-155 tumor models. **Conclusion:** This study demonstrated that ^{64}Cu-NOTA-F(ab′)$_2$-obinutuzumab had a rapid and sustained tumor uptake in CD20-positive lymphoma with high contrast, which could enable noninvasive evaluation of CD20 levels in the clinic.

Key Words: F(ab′)$_2$; obinutuzumab; CD20; PET; lymphoma

J Nucl Med 2021; 62:372–378
DOI: 10.2967/jnumed.120.246595

Non-Hodgkin lymphoma is a class of heterogeneous lymphoid hematologic malignancies primarily with B-cell origin (B-non-Hodgkin lymphoma, about 85%) (*1*). CD20 is highly expressed in malignant B cells, especially B-non-Hodgkin lymphoma, and is considered an important diagnosis biomarker and therapeutic target (*2*). Monoclonal antibodies (mAbs) targeting CD20 have high therapeutic efficacy in the clinic. Rituximab, a first-generation CD20-targeted mAb, has saved millions of patients with B-cell malignancies. However, this chimeric antibody may induce immunogenicity leading to treatment failure (*3*). Obinutuzumab is a next-generation humanized and glycoengineered type II IgG1 mAb targeting CD20. It recognizes a unique epitope and significantly increases direct cell death compared with rituximab (*4*).

Expression of CD20 is a marker for evaluating treatment efficacy. Although pathologic results are the gold standard, acquiring samples is typically invasive and inconvenient. ^{18}F-FDG PET/CT is currently the primary technique for therapeutic evaluation of lymphoma. However, ^{18}F-FDG is a nonspecific agent, which complicates diagnosis and may create false results. Immuno-PET is a noninvasive molecular imaging method that uses a radiolabeled antibody (*5,6*) to visualize a specific marker, as was previously demonstrated with ^{89}Zr-labeled obinutuzumab, which successfully assessed CD20 expression in murine tumor models (*7*).

Received Apr. 7, 2020; revision accepted Jul. 9, 2020.
For correspondence or reprints contact any of the following:
Weibo Cai, University of Wisconsin–Madison, 1111 Highland Ave., Room 7137, Madison, WI 53705.
E-mail: wcai@uwhealth.org
Xiaojie Xu, 27 Taiping Rd., Beijing, 100850, China.
E-mail: miraclexxj@126.com
Dawei Jiang, 1277 Jiefang Ave., Wuhan, Hubei 430022, China.
E-mail: daweijiang@hust.edu.cn
Lei Kang, 8 Xishiku St., Xicheng Dist., Beijing, 100034, China.
E-mail: kanglei@bjmu.edu.cn
*Contributed equally to this work.
Published online Aug. 21, 2020.

F(ab) (~50 kDa) and F(ab′)$_2$ (~110 kDa) fragments from an IgG antibody (~150 kDa) can be produced by enzymatic digestion, and they retain the same antigen-binding site and immunologic binding activity as the intact antibody (*8*). Imaging agents based on intact antibodies are frequently limited by their long circulation half-life in the body and slow tumor penetration, leading to delayed peak tumor uptake at several days after injection (*5*). In our previous study, immuno-PET imaging with a ^{89}Zr-labeled CD38-targeted mAb (daratumumab) exhibited a specific binding ability for delineating lymphoma tumors in vivo (*9*). However, the tumor uptake peaked at 5 d after injection and the radioactivity in the blood remained high up to 4 d. Since F(ab′)$_2$ fragments are eliminated from blood more rapidly than intact mAbs while retaining high binding affinity (*8,10*), it may be propitious to prepare F(ab′)$_2$ fragments of obinutuzumab for PET imaging of lymphoma. In this study, we aimed to develop F(ab′)$_2$-obinutuzumab for immuno-PET imaging of CD20 in lymphoma murine models with a shortened imaging window.

MATERIALS AND METHODS

Preparation of F(ab′)$_2$ Fragments

F(ab′)$_2$-obinutuzumab was prepared using the IgG-degrading enzyme of *Streptococcus pyogenes* (IdeS) protease kit (Promega) and purified by removing the Fc portion. In brief, obinutuzumab (Roche) was incubated with IdeS protease for 30 min at 37°C in the digestion buffer (50 mM sodium phosphate, 150 mM NaCl, pH 6.6). The digested products were then incubated with Magne Protein A beads (Promega) for 1 h and centrifuged. The Fc portion attached to the beads was removed in the sediment, whereas the purified F(ab′)$_2$ stayed in the supernatant. The products were evaluated by sodium dodecyl sulfate polyacrylamide gel electrophoresis (SDS-PAGE) and high-performance liquid chromatography (HPLC). SDS-PAGE was conducted on a 12% gel under 120 V for 1 h. The nonreducing gel was stained by Coomassie brilliant blue at room temperature (RT). HPLC was performed on a Dionex UltiMate3000 Chromeleon system (ThermoFisher). F(ab′)$_2$ of an isotype IgG (ThermoFisher) was prepared as a control.

Stability Test

F(ab′)$_2$-obinutuzumab (4.58 μM) was incubated in phosphate-buffered saline (PBS) or 10% of fetal bovine serum (Invitrogen) at 37°C for 2, 4, 6, 12, and 24 h, respectively. The solvents were analyzed by SDS-PAGE using the same condition as described above.

Radiolabeling

F(ab′)$_2$-obinutuzumab was labeled by ^{64}Cu (half-life, 12.7 h) after being conjugated with NOTA (Macrocyclics). In brief, F(ab′)$_2$-obinutuzumab was incubated with NOTA for 2 h at RT in a carbonate buffer (pH 9.0), and the molar ratio of F(ab′)$_2$ to NOTA was 1:10–20. NOTA-F(ab′)$_2$-obinutuzumab was purified using PD-10 columns (GE Healthcare) with PBS as the mobile phase. For radiolabeling with ^{64}Cu, NOTA-F(ab′)$_2$-obinutuzumab was incubated with $^{64}CuCl_2$ in sodium acetate buffer (pH 5.5) for 1 h at 37°C and purified with PD-10 columns. The ratio of NOTA-F(ab′)$_2$ to $^{64}CuCl_2$ was no less than 0.68 μg/MBq. A similar protocol was used to prepare ^{64}Cu-labeled F(ab′)$_2$-IgG.

Cell Culture and Xenograft Model

Five lymphoma cell-lines including Ramos, Daudi, OCI-LY10, Raji, and CCL-155 were purchased from American Type Culture Collection. Cells were cultured in RPMI 1640 medium supplemented with 10% fetal bovine serum and 1% penicillin/streptomycin (Invitrogen) at 37°C with 5% CO_2.

Animal studies were approved by the Wisconsin University Institutional Animal Care and Use Committee. Immunodeficient male CB-17 SCID mice (4–6 wk old; Envigo) were used to establish xenograft tumor models with Ramos and CCL-155 cells. The lower right flank of each mouse was subcutaneously injected with 1×10^7 cells suspended in 200 μL of Matrigel (Invitrogen). Animal health and tumor volumes were monitored every other day.

Western Blotting

Western blotting was used to screen the cellular CD20 expression. Collected proteins were loaded into the 4%–12% Bolt Bis-Tris Plus gel (ThermoFisher), electrophorized for 60 min under 110 V at 4°C, and transferred to a nitrocellulose membrane. The membrane was blocked with Odyssey blocking buffer (LI-COR) at RT for 1 h and incubated with mouse antihuman CD20 (1:1,000) and rabbit antihuman β-actin (1:2,000) primary antibodies (Novus Biologicals) overnight at 4°C. After washing with PBS with polysorbate 20, the membrane was incubated with donkey antimouse IRDye 800CW and goat antirabbit IRDye 680RD secondary antibodies (LI-COR) for scanning and analysis using Odyssey infrared imaging system (LI-COR).

Immunofluorescence Cell Staining

NHS-fluorescein (ThermoFisher) was conjugated with F(ab′)$_2$ at a molar ratio of 1:3 in a carbonate buffer (pH 9.0) for 2 h. The fluorescent product was purified using PD-10 columns by removing excess dye. When Ramos cells were cultured in 6-well plates at a confluence of 40%, fluorescein-F(ab′)$_2$ were incubated in the medium at 10 ng/mL overnight. Cells were then collected and treated with 4′,6-diamidino-2-phenylindole–containing HardSet mounting medium (Vector Laboratories). Imaging was performed using a Nikon confocal system (A1RS).

Flow Cytometry

Ramos and CCL-155 cells were incubated with F(ab′)$_2$-obinutuzumab, obinutuzumab, and IgG (10 μg/mL) in flow cytometry staining buffer solution (eBioscience) at 1×10^6 cells/mL for 30 min at RT. The cells were washed with cold PBS (pH 7.4) and then incubated with a fluorescein-labeled goat antihuman IgG F(ab′)$_2$ secondary antibody (3 μg/mL; ThermoFisher) for 20 min at RT. After being washed, the cells were analyzed using a FACSCanto II analyzer (BD Biosciences). Fluorescein intensities were processed with FlowJo software (Tree Star).

Enzyme-Linked Immunosorbent Assay

An in-cell indirect enzyme-linked immunosorbent assay was used to test the binding affinity of F(ab′)$_2$ in Ramos and CCL-155 cells. Obinutuzumab and nonspecific IgG were used as controls. In brief, various concentrations of antibodies (0–134 nmol/L) were incubated with 1×10^5 cells for 1 h at RT in a 96-well culture plate ($n = 3$). The cells were centrifuged at 1,650 rpm for 5 min and washed with cold PBS. A horseradish peroxidase–coupled antihuman IgG F(ab′)$_2$ secondary antibody (Abcam) was incubated (1:5,000) for 30 min at RT. After washing, a peroxidase substrate (Abcam) was added and then stopped by an equal volume of H_2SO_4 solution (2 M). Spectrophotometric readings were made at 450 nm using a Synergy H1 reader (BioTek). Maximum binding ability (B_{max}) and affinity constants (K_D) were calculated using GraphPad Prism software.

PET Imaging

PET imaging was performed when the diameter of tumors reached about 10 mm. Tumor-bearing mice were intravenously injected with 5–10 MBq of ^{64}Cu-labeled F(ab′)$_2$-obinutuzumab or F(ab′)$_2$-IgG. After being anesthetized with 2% isoflurane, the mice were imaged on an Inveon small-animal PET/CT scanner (Siemens) at 10 min, 4 h, 12 h, 24 h, and 48 h after injection. Twenty million coincidence events were collected at each time per mouse, and images were reconstructed using a 3-dimensional workstation. Regions of interest for the tumor, heart, liver, kidneys, bone, and muscle were quantified with the Inveon Research Workspace software.

Biodistribution

After the terminal imaging time-point, the mice were euthanized by carbon dioxide asphyxiation. Major organs and tissues, including the tumor, heart, liver, spleen, lung, kidneys, stomach, intestine, pancreas, tail, skin, muscle, bone, brain, and blood, were harvested and weighed, and activity was then measured with an automated γ-counter (PerkinElmer). The biodistribution data are presented as percentage injected dose per gram of tissue (%ID/g).

Immunofluorescence Tissue Staining

Immunofluorescence staining was performed following established protocols (*9,11,12*). After blocking with 10% donkey serum for 60 min, tissue slides were incubated with rabbit antihuman anti-CD20 (1:400; Novus Biologicals) and rat antimouse anti-CD31 (1:100; ThermoFisher) primary antibodies overnight at 4°C. The slides were washed and stained with AlexaFluor488-labeled goat antirabbit and Cy3-labeled donkey antirat secondary antibodies (ThermoFisher). Slides were mounted with 4′,6-diamidino-2-phenylindole–containing HardSet mounting medium and imaged with a Nikon A1RS confocal microscope.

Statistical Analysis

All quantitative data are presented as mean ± SD. The Student *t* test was used for comparisons between groups. *P* values of less than 0.05 were considered statistically significant.

RESULTS

Preparation of ^{64}Cu-Labeled F(ab′)$_2$

F(ab′)$_2$ was prepared by digesting intact mAbs using IdeS protease and purified with magnetic beads (Fig. 1A). SDS-PAGE showed the molecular weight of obinutuzumab to be approximately 150 kDa, whereas F(ab′)$_2$-obinutuzumab was approximately 100 kDa, consistent with the theoretic molecular weight (Fig. 1B). HPLC showed 1 main peak of F(ab′)$_2$-obinutuzumab locating after the obinutuzumab peak (Fig. 1C), indicating that F(ab′)$_2$-obinutuzumab was successfully prepared with high purity. ^{64}Cu-labeled F(ab′)$_2$-obinutuzumab achieved a yield of more than 90% (n = 6). Purified ^{64}Cu-NOTA-F(ab′)$_2$-obinutuzumab had a radiochemical purity of more than 98% and a specific activity of 56.3 ± 7.9 MBq/mg. SDS-PAGE showed that the bands of F(ab′)$_2$-obinutuzumab were clearly seen without diffusion over 24 h in PBS or 10% fetal bovine serum, indicating excellent in vitro stability (Fig. 1D).

Cellular Screening and Binding Affinity

In Western blotting, Ramos showed the highest expression of CD20 whereas CLL-155 showed the lowest (Fig. 2A). Visualized by confocal microscopy, strong binding from fluorescein-F(ab′)$_2$-obinutuzumab was found on Ramos cells. In contrast, a nonspecific signal was observed for fluorescein-F(ab′)$_2$-IgG or fluorescein dye only (Fig. 2B). Flow cytometry showed a strong signal shift after incubation of F(ab′)$_2$-obinutuzumab and obinutuzumab with Ramos cells, suggesting specific binding of F(ab′)$_2$-obinutuzumab and obinutuzumab with CD20 (Fig. 2C). Cell-binding results from enzyme-linked immunosorbent assay indicated that F(ab′)$_2$-obinutuzumab and obinutuzumab had high binding affinity with Ramos cells but only nonspecific binding with CCL-155 cells. The K_D of F(ab′)$_2$-obinutuzumab and obinutuzumab was 3.7 ± 0.6 nM and 1.5 ± 0.4 nM, respectively, whereas both had a B_{max} of 0.22 ± 0.01 pmol and the receptor density of Ramos cells was about 1.33 × 10^6 per cell (Fig. 2D).

PET Imaging and Quantitative Analysis

Maximum-intensity-projection images of ^{64}Cu-NOTA-F(ab′)$_2$-obinutuzumab and ^{64}Cu-NOTA-F(ab′)$_2$-IgG are displayed in Figure 3. Ramos tumor showed high tracer uptake and excellent contrast as early as 4 h and peaked at 12 h after injection of ^{64}Cu-NOTA-F(ab′)$_2$-obinutuzumab. In contrast, ^{64}Cu-NOTA-F(ab′)$_2$-IgG could not delineate the tumor at any time point. CCL-155 tumors showed a near-uniform tumor-to-background uptake of ^{64}Cu-NOTA-F(ab′)$_2$-obinutuzumab. Both F(ab′)$_2$-obinutuzumab and F(ab′)$_2$-IgG had high uptake in the kidneys and bladder due to clearance via the urinary system. Tracer uptake in large blood vessels and blood-rich organs decreased significantly after 4 h, suggesting that F(ab′)$_2$ had an optimal in vivo blood clearance.

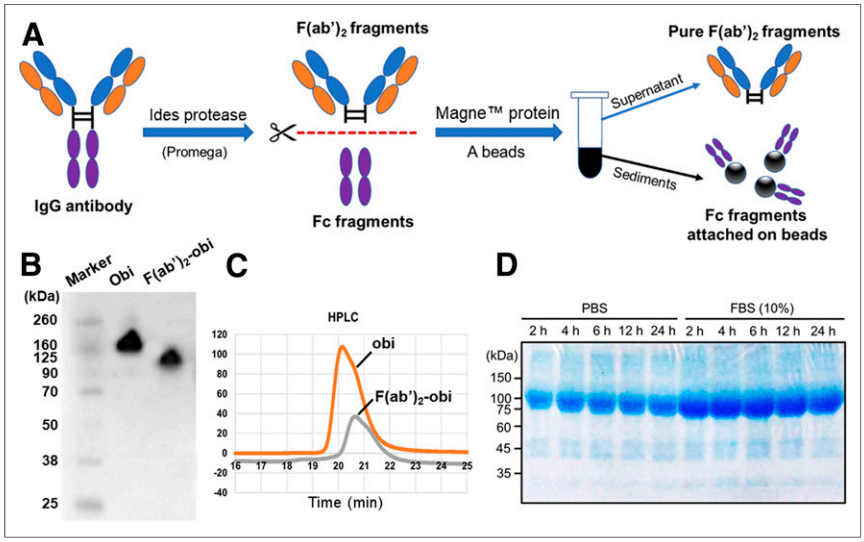

FIGURE 1. Preparation and verification of F(ab′)$_2$. (A) F(ab′)$_2$ fragments were prepared using IdeS protease and purified using magnetic protein A beads. (B) SDS-PAGE showed size of obinutuzumab (obi) and F(ab′)$_2$-obinutuzumab. (C) HPLC showed peak of F(ab′)$_2$-obinutuzumab right after its intact form. (D) SDS-PAGE displayed good stability of F(ab′)$_2$-obinutuzumab after incubation in PBS or 10% fetal bovine serum over 24 h. FBS = fetal bovine serum.

Quantitative region-of-interest analysis (Fig. 4A) observed high and sustained tumor uptake (>7 %ID/g) for ^{64}Cu-NOTA-F(ab′)$_2$-obinutuzumab in the Ramos model. The highest tumor uptake for ^{64}Cu-NOTA-F(ab′)$_2$-obinutuzumab (9.08 ± 1.67 %ID/g) occurred at 12 h after injection in the Ramos model and was significantly higher than in the CCL-155 model (2.78 ± 0.62 %ID/g, P = 0.000001, n = 4). In comparison, the peak tumor uptake of ^{64}Cu-NOTA-F(ab′)$_2$-IgG was significantly lower than that of ^{64}Cu-NOTA-F(ab′)$_2$-obinutuzumab (P = 0.000001), at only 1.93 ± 0.26 %ID/g (n = 4). In all 3 groups, uptake in the kidneys peaked between 4 and 12 h and then decreased. Uptake in other organs (heart, liver, bone, and muscle) was highest immediately after injection and then decreased over time. Tumor-to-blood (T/B) and tumor-to-muscle (T/M) ratios (Fig. 4B) increased gradually and peaked at 7.32 ± 1.61 and 21.88 ± 8.99 at 48 h, respectively, after injection of ^{64}Cu-NOTA-F(ab′)$_2$-obinutuzumab in the Ramos model. The highest T/B ratios in the F(ab′)$_2$-IgG

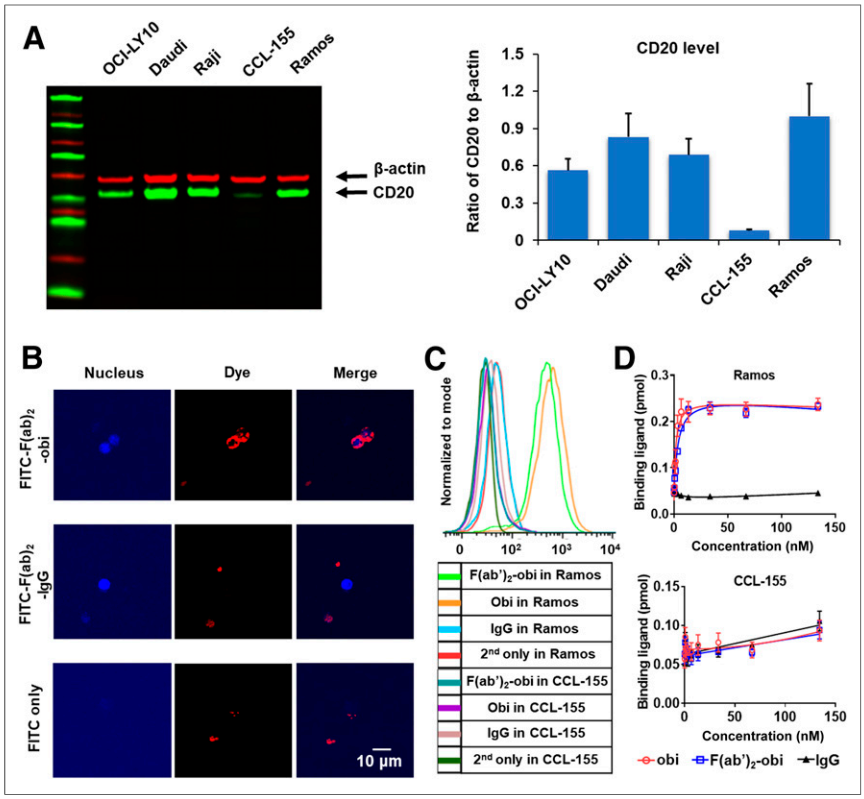

FIGURE 2. Cellular evaluation of CD20 expression and binding affinity. (A) Western blotting showed CD20 expression of 5 different lymphoma cells. (B) Confocal microscopy showed strong binding of F(ab′)$_2$-obinutuzumab with Ramos cells but not control samples. (C) Flow cytometry confirmed specific binding of F(ab′)$_2$-obinutuzumab and obinutuzumab with Ramos cells. (D) Enzyme-linked immunosorbent assay indicated that F(ab′)$_2$-obinutuzumab had high binding affinity with Ramos cells (K_D = 3.7 ± 0.6 nM, B_{max} = 0.22 ± 0.01 pmol).

group (1.09 ± 0.33) and the CCL-155 group (1.50 ± 0.48) were significantly lower (P = 0.000002 and 0.000004, respectively). These quantitative results indicated that ^{64}Cu-NOTA-F(ab′)$_2$-obinutuzumab could specifically visualize differential expression of CD20 in vivo.

Ex Vivo Biodistribution

Overall, the biodistribution results at 48 h (n = 4) corroborated the above region-of-interest analysis (Fig. 5). Tumor uptake of F(ab′)$_2$-obinutuzumab was significantly higher in the Ramos group (6.07 ± 0.57 %ID/g) than in the CCL-155 group (1.14 ± 0.21 %ID/g, P = 0.000001), and higher than the tumor uptake of F(ab′)$_2$-IgG in the Ramos group (0.80 ± 0.18 %ID/g, P = 0.000001). Renal uptake in the 3 groups (15.32 ± 0.88, 14.34 ± 1.03, and 12.36 ± 3.19 %ID/g in the F(ab′)$_2$-obinutuzumab in the Ramos group, F(ab′)$_2$-obinutuzumab in the CCL-155 group, and F(ab′)$_2$-IgG in the Ramos group, respectively) did not significantly differ ($P > 0.05$). Blood retention of F(ab′)$_2$-obinutuzumab in the Ramos model (0.45 ± 0.11 %ID/g) was lower than in the other groups (0.76 ± 0.10 and 0.86 ± 0.09 %ID/g in the F(ab′)$_2$-obinutuzumab in the CCL-155 and F(ab′)$_2$-IgG in Ramos groups, respectively, P = 0.03 and 0.02), probably because of higher tumor uptake. The biodistribution of all other organs and tissues did not significantly differ ($P > 0.05$).

Tumor Tissue Staining

Ramos and CCL-155 tumors were removed and stained for CD20 expression (Fig. 6). Ramos tumor showed a strong CD20 signal (green) around the cell membrane in tumors, whereas CCL-155 showed a very weak signal, as correlated well with PET observations. CD31 staining indicated rich angiogenesis in both tumors.

DISCUSSION

CD20 is overexpressed in 90% of B-cell lymphomas, which account for about 85% of all lymphomas. Among Hodgkin lymphomas, 20%–40% are also CD20-positive (*7*). Evaluation of CD20 expression is important to assess treatment efficacy. Although rituximab, a first-generation anti-CD20 mAb, has long been publicly recognized for its therapeutic efficacy in lymphoma, its potential as a specific imaging agent targeting CD20 has only recently been investigated (*13,14*). Obinutuzumab is the first type II, glycoengineered anti-CD20 humanized mAb. Compared with rituximab, obinutuzumab is less immunogenic, is more effective at inducing direct cell death, and has a higher binding affinity (*15*). Because of these advantages, obinutuzumab would be a better choice for CD20-specific immuno-PET imaging.

Immuno-PET combines the specificity of antibodies with the sensitivity of PET imaging, facilitating noninvasive evaluation of unique phenotypes of tumors in vivo (*6,16*). The large size of intact antibodies (~150 kDa) potentially hinders the clinical translation of antibody-based imaging agents for several reasons. First, delayed peak tumor uptake in the days after administration limits the possibility of imaging on the same day as the injection. In previous studies, ^{89}Zr-labeled rituximab or obinutuzumab required up to 7 d to reach maximal uptake in CD20-positive animal models (*7,13*). When ^{89}Zr-labeled rituximab was used in patients with diffuse large B-cell lymphoma, its optimal tumor uptake was also at 6 d after injection (*14*). Second, intact antibodies have slow blood clearance and relatively high uptake in the liver from hepatic clearance. These characteristics decrease the target contrast and worsen imaging quality. Third, studying the long-term biodistribution of intact antibodies requires radionuclides with longer half-lives, such as ^{89}Zr (78.4 h) and ^{124}I (100.8 h). This will typically expose patients to more radiation (*17*). Because of these disadvantages, alternative immuno-PET imaging probes must be developed for successful clinical translation.

F(ab′)$_2$ fragments, lacking the Fc portion of mAbs, have a shorter blood circulation and interact less with complements than do intact mAbs (*18*). According to a previous study, the highest uptake (44.4 ± 7.6 %ID/g) of ^{89}Zr-obinutuzumab in Raji tumors (CD20-positive) occurred at 7 d (*7*). In our study, the highest ^{64}Cu-NOTA-F(ab′)$_2$-obinutuzumab tumor uptake (9.1 ± 1.7 %ID/g) occurred at 12 h after injection in the Ramos model—much earlier than for ^{89}Zr-obinutuzumab. By comparing the cellular binding affinity of F(ab′)$_2$-obinutuzumab and obinutuzumab, our study found that they had specific binding with Ramos cells, with similar B_{max} (0.22 ± 0.01 pmol) and high K_D values (<4 nM). Importantly, our study found that similar tumor uptake (8.3 ± 2.0 %ID/g)

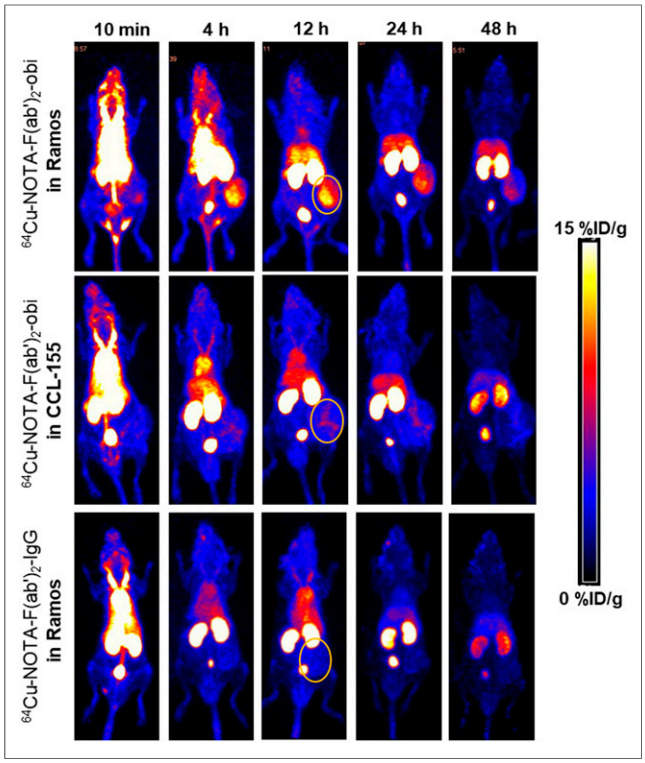

FIGURE 3. PET imaging of ^{64}Cu-NOTA-F(ab′)$_2$-obinutuzumab and ^{64}Cu-NOTA-F(ab′)$_2$-IgG in Ramos and CCL-155 murine models. ^{64}Cu-NOTA-F(ab′)$_2$-obinutuzumab could visualize Ramos tumor clearly after 4 h after injection. In contrast, ^{64}Cu-NOTA-F(ab′)$_2$-IgG barely delineated tumor. Besides, CCL-155 tumor could not be shown after injection of ^{64}Cu-NOTA-F(ab′)$_2$-obinutuzumab. Circles indicate tumors.

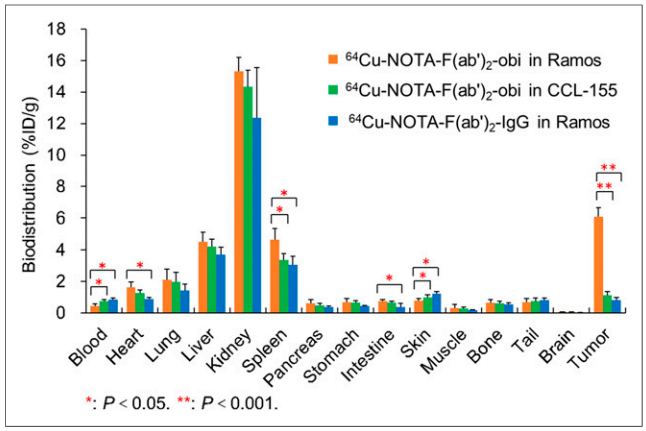

FIGURE 5. Biodistribution results at 48 h after injection. Tumor uptake of ^{64}Cu-NOTA-F(ab′)$_2$-obinutuzumab in Ramos group was significantly higher than that of ^{64}Cu-NOTA-F(ab′)$_2$-IgG in Ramos group and ^{64}Cu-NOTA-F(ab′)$_2$-obinutuzumab in CCL-155 group ($P < 0.001$). Renal uptake was higher than uptake in other organs in the 3 groups, whereas blood uptake was below 1 %ID/g in all.

can be obtained at a time point as early as 4 h after injection of ^{64}Cu-NOTA-F(ab′)$_2$-obinutuzumab. The rapid and prominent tumor uptake make ^{64}Cu-NOTA-F(ab′)$_2$-obinutuzumab suitable for clinical translation by enabling same-day imaging and improving the imaging quality compared with the intact mAb. Compared with F(ab), F(ab′)$_2$ typically has a longer circulation half-life and higher tumor uptake. Mendler et al. (*19*) prepared a ^{125}I-labeled F(ab) of ofatumumab that is a full human CD20 mAb but found that tumor uptake was low (1.3 ± 0.1 %ID/g at 6 h and 0.2 %ID/g at 24 h). Our results suggested that F(ab′)$_2$ may be a better choice for tumor imaging than F(ab). ^{64}Cu has a half-life of 12.7 h and is an excellent match to the time required for peak tumor uptake in this study.

Another advantage of F(ab′)$_2$ for imaging is the better tumor contrast stemming from faster blood clearance (*20*). In our study, the T/B ratio reached 7.3 ± 1.6 at 2 d. In comparison, the same T/B ratio was obtained 7 d after injection of ^{89}Zr-obinutuzumab (*7*). Compared with ^{89}Zr-rituximab, ^{64}Cu-NOTA-F(ab′)$_2$-obinutuzumab achieved a high T/M ratio (21.9 ± 9.0) as early as 2 d after injection (*13*). Moreover, both ^{64}Cu-NOTA-F(ab′)$_2$-obinutuzumab in CCL-155 tumors and ^{64}Cu-NOTA-F(ab′)$_2$-IgG in Ramos tumors showed significantly lower tumor contrast at 48 h after injection (respectively: T/B = 1.5 ± 0.5 and 1.1 ± 0.3; T/M = 7.9 ± 4.0 and 4.6 ± 2.4). Although ^{68}Ga-labeled F(ab) and F(ab′)$_2$ for rituximab have previously been developed, they were evaluated at only the cellular level (*21*). Therefore, our study confirmed that ^{64}Cu-labeled F(ab′)$_2$-obinutuzumab is promising for evaluating the differential CD20 expression of lymphoma noninvasively.

A concise understanding of the properties of ^{64}Cu-labeled F(ab′)$_2$-obinutuzumab will guide future applications and clinical translation to ensure its in vivo performance. Generally, favorable radiolabeling efficiency, high specific activity, and good stability are essential (*6*). Cooper et al. (*22*) compared the labeling and the

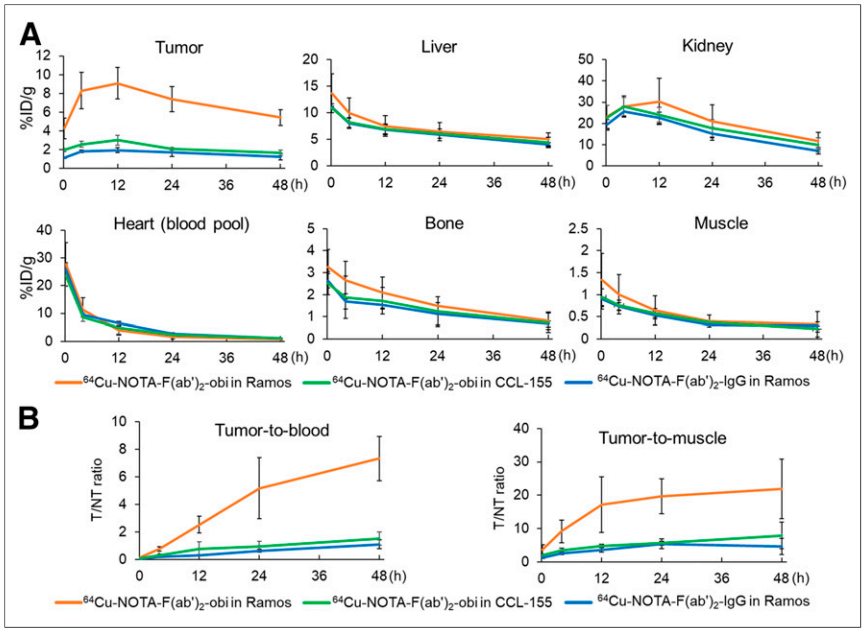

FIGURE 4. Semiquantitative analysis of PET images. (A) Peak tumor uptake (9.1 ± 1.7 %ID/g) was obtained at 12 h after injection of ^{64}Cu-NOTA-F(ab′)$_2$-obinutuzumab in Ramos group, which was significantly higher than F(ab′)$_2$-IgG in Ramos group (2.8 ± 0.6 %ID/g) and F(ab′)$_2$-obinutuzumab in CCL-155 group (1.9 ± 0.3 %ID/g, $P < 0.001$). (B) T/B and T/M ratios of ^{64}Cu-NOTA-F(ab′)$_2$-obinutuzumab in Ramos group were significantly higher than those of control groups ($P < 0.05$). T/NT = tumor-to-nontumor.

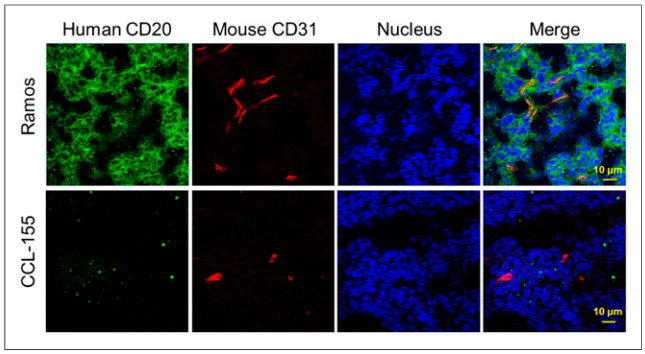

FIGURE 6. Immunofluorescence staining of tumor tissues. Strong CD20 expression (green signals) was found throughout Ramos tumors, whereas near-background signals were shown around CCL-155 tumors. CD31 signals represent angiogenesis.

in vitro and in vivo characteristics of 8 commonly used chelators for ^{64}Cu-radiolabeling and concluded that NOTA had significant advantages over the other tested chelators. NOTA-chelated rituximab could be radiolabeled rapidly at RT with high serum stability for over 48 h. To provide homogeneous, uniform, and predictable products, site-specific conjugation methods have been used in the preparation of radiolabeled antibodies, via the modification of endogenous sites on antibodies (*23*), addition of cysteine residues (*5,24*) and use of some click chemistry pairs (*25*).

To image CD20 in vivo, some antibody-derived imaging probes with smaller sizes have been developed. Olafsen et al. (*26*) developed an 80-kDa minibody and a modified scFv-Fc (105 kDa) from rituximab. The ^{124}I-minibody reached a maximum tumor uptake of 12.9 ± 3.4 %ID/g at 21 h after injection in a CD20-positive lymphoma murine model. The T/B ratio was only 4.8 ± 1.5, which is significantly lower than that for F(ab′)$_2$-obinutuzumab in our study. Krasniqi et al. (*27*) developed camelid single-domain antibody fragments with a very small size (<15 kDa). The T/B ratio was also drastically lower than in our study but was acceptable (3.7 ± 0.7) at 1.5 h after injection of ^{68}Ga-NOTA single-domain antibody fragments. However, tumor uptake was only 3.4 ± 1.3 %ID/g and decreased to 1.6 ± 0.1 %ID/g at 6 h after injection. Another immuno-PET study used ^{89}Zr- or ^{124}I-labeled cysteine-diabodies derived from obinutuzumab and found that ^{89}Zr-cysteine-diabody yielded greater tumor uptake (4.9 ± 0.3 %ID/g at 24 h) and T/B ratios (14.4 ± 1.5 at 24 h) than did ^{124}I-labeled tracers (*24*). In our study, ^{64}Cu-labeled F(ab′)$_2$ is also bivalent and features the residualizing PET isotope. Compared with ^{89}Zr-cysteine-diabody, the tumor uptake of F(ab′)$_2$ showed a comparable level (8.3 ± 1.9 %ID/g vs. ~9 %ID/g) at 4 h but a higher level (7.4 ± 1.4 %ID/g vs. 4.9 ± 0.3 %ID/g) at 24 h, whereas the T/B ratio at 24 h was less (5.2 ± 2.2 vs. 14.4 ± 1.5). Since their K_D values are in the similar low-nanomolar range of less than 4 nM, the difference in tumor uptake might be relative to the larger size of F(ab′)$_2$ and the different CD20 level of Ramos cells. Because of the residualizing nature of ^{89}Zr, ^{89}Zr-cysteine-diabody showed higher nonspecific uptake, especially in the kidneys, than ^{124}I-labeled tracer. Although ^{64}Cu-labeled F(ab′)$_2$ showed high nontarget uptake in the kidneys (21.0 ± 7.8 %ID/g at 24 h), it was much lower than that for ^{89}Zr-cysteine-diabody (106.8 ± 2.5 %ID/g at 24 h), suggesting better contrast of the kidneys.

Although antibody fragments can significantly enhance blood clearance and tumor contrast, these small tracers typically undergo rapid renal filtration and elimination (*16*). Radiolabeled agents of similar or smaller size would also have high renal uptake (*21*). These lead to high kidney accumulation and may induce nephrotoxicity. Some strategies have been used to reduce renal uptake. Conjugation of polyethylene glycol to antibody fragments was used to increase the molecular weight beyond the cutoff for glomerular filtration but increased circulation half-life (*28*). A pretargeting strategy separately administering the antibody-based probe and the radionuclide have also been used to decrease renal radionuclide accumulation (*29*). However, pretargeting requires optimization, which creates difficulty and also typically reduces tumor uptake. Therefore, the optimal size of mAb fragments using feasible methods requires further investigation in the future.

CONCLUSION

This study used a ^{64}Cu-labeled F(ab′)$_2$ of obinutuzumab to visualize the differential expression of CD20 in vivo. ^{64}Cu-NOTA-F(ab′)$_2$-obinutuzumab was found to be a specific and efficient imaging agent for CD20-positive tumors. Furthermore, ^{64}Cu-NOTA-F(ab′)$_2$-obinutuzumab showed rapid and persistent tumor uptake with a low background, which may allow for same-day immuno-PET imaging in future clinical applications.

DISCLOSURE

This work was supported by the University of Wisconsin–Madison, the National Institutes of Health (P30CA014520), the National Natural Science Foundation of China (81871385), the PKU Medicine-X Youth Program (PKU2020LCXQ007), and Open Funding Project of the State Key Laboratory of Biochemical Engineering (2020KF-01). No other potential conflict of interest relevant to this article was reported.

KEY POINTS

QUESTION: Can F(ab′)$_2$ produced from obinutuzumab be used to accurately visualize differentiated CD20 expression of lymphoma?

PERTINENT FINDINGS: This work successfully produced ^{64}Cu-NOTA-F(ab′)$_2$-obinutuzumab, and immuno-PET imaging validated it as a specific and efficient tracer for CD20-positive tumors, with excellent tumor contrast.

IMPLICATIONS FOR PATIENT CARE: To characterize the dynamics of CD20-positive lymphoma, immuno-PET imaging using anti-CD20 F(ab′)$_2$ fragments can help refine clinical cancer diagnoses when F(ab′)$_2$ tracers are highly useful as efficacious same-day imaging tracers.

REFERENCES

1. Swerdlow SH, Campo E, Pileri SA, et al. The 2016 revision of the World Health Organization classification of lymphoid neoplasms. *Blood.* 2016;127:2375–2390.
2. Shanehbandi D, Majidi J, Kazemi T, Baradaran B, Aghebati-Maleki L. Cd20-based immunotherapy of b-cell derived hematologic malignancies. *Curr Cancer Drug Targets.* 2017;17:423–444.
3. Freeman CL, Sehn LH. A tale of two antibodies: obinutuzumab versus rituximab. *Br J Haematol.* 2018;182:29–45.
4. Illidge T, Klein C, Sehn LH, Davies A, Salles G, Cartron G. Obinutuzumab in hematologic malignancies: lessons learned to date. *Cancer Treat Rev.* 2015; 41:784–792.
5. Zettlitz KA, Tavare R, Tsai WK, et al. ^{18}F-labeled anti-human CD20 cys-diabody for same-day immunoPET in a model of aggressive B cell lymphoma in human CD20 transgenic mice. *Eur J Nucl Med Mol Imaging.* 2019;46:489–500.

6. Wei W, Rosenkrans ZT, Liu J, Huang G, Luo QY, Cai W. ImmunoPET: concept, design, and applications. *Chem Rev.* 2020;120:3787–3851.
7. Yoon JT, Longtine MS, Marquez-Nostra BV, Wahl RL. Evaluation of next-generation anti-CD20 antibodies labeled with ^{89}Zr in human lymphoma xenografts. *J Nucl Med.* 2018;59:1219–1224.
8. Hong H, Zhang Y, Orbay H, et al. Positron emission tomography imaging of tumor angiogenesis with a $^{61/64}$Cu-labeled F(ab′)(2) antibody fragment. *Mol Pharm.* 2013;10:709–716.
9. Kang L, Jiang D, England CG, et al. ImmunoPET imaging of CD38 in murine lymphoma models using ^{89}Zr-labeled daratumumab. *Eur J Nucl Med Mol Imaging.* 2018;45:1372–1381.
10. Luo H, Hernandez R, Hong H, et al. Noninvasive brain cancer imaging with a bispecific antibody fragment, generated via click chemistry. *Proc Natl Acad Sci USA.* 2015;112:12806–12811.
11. England CG, Ehlerding EB, Hernandez R, et al. Preclinical pharmacokinetics and biodistribution studies of ^{89}Zr-labeled pembrolizumab. *J Nucl Med.* 2017;58: 162–168.
12. Li S, England CG, Ehlerding EB, et al. ImmunoPET imaging of CD38 expression in hepatocellular carcinoma using ^{64}Cu-labeled daratumumab. *Am J Transl Res.* 2019;11:6007–6015.
13. Natarajan A, Habte F, Gambhir SS. Development of a novel long-lived immunoPET tracer for monitoring lymphoma therapy in a humanized transgenic mouse model. *Bioconjug Chem.* 2012;23:1221–1229.
14. Jauw YW, Zijlstra JM, de Jong D, et al. Performance of ^{89}Zr-labeled-rituximab-PET as an imaging biomarker to assess CD20 targeting: a pilot study in patients with relapsed/refractory diffuse large B cell lymphoma. *PLoS One.* 2017;12: e0169828.
15. Mössner E, Brunker P, Moser S, et al. Increasing the efficacy of CD20 antibody therapy through the engineering of a new type II anti-CD20 antibody with enhanced direct and immune effector cell-mediated B-cell cytotoxicity. *Blood.* 2010;115: 4393–4402.
16. England CG, Rui L, Cai W. Lymphoma: Current status of clinical and preclinical imaging with radiolabeled antibodies. *Eur J Nucl Med Mol Imaging.* 2017;44:517–532.
17. Zhang Y, Hong H, Cai W. PET tracers based on zirconium-89. *Curr Radiopharm.* 2011;4:131–139.
18. Valedkarimi Z, Nasiri H, Aghebati-Maleki L, Abdolalizadeh J, Esparvarinha M, Majidi J. Production and characterization of anti-human igg F(ab′)2 antibody fragment. *Hum Antibodies.* 2018;26:171–176.
19. Mendler CT, Friedrich L, Laitinen I, et al. High contrast tumor imaging with radio-labeled antibody Fab fragments tailored for optimized pharmacokinetics via pasylation. *MAbs.* 2015;7:96–109.
20. Fu R, Carroll L, Yahioglu G, Aboagye EO, Miller PW. Antibody fragment and affibody immunoPET imaging agents: radiolabelling strategies and applications. *ChemMedChem.* 2018;13:2466–2478.
21. Suman SK, Kameswaran M, Pandey U, Sarma HD, Dash A. Preparation and preliminary bioevaluation studies of ^{68}Ga-NOTA-rituximab fragments as radioimmunoscintigraphic agents for non-Hodgkin lymphoma. *J Labelled Comp Radiopharm.* 2019;62:850–859.
22. Cooper MS, Ma MT, Sunassee K, et al. Comparison of ^{64}Cu-complexing bifunctional chelators for radioimmunoconjugation: labeling efficiency, specific activity, and in vitro/in vivo stability. *Bioconjug Chem.* 2012;23:1029–1039.
23. Wu AM. Engineered antibodies for molecular imaging of cancer. *Methods.* 2014;65:139–147.
24. Zettlitz KA, Tavare R, Knowles SM, Steward KK, Timmerman JM, Wu AM. Immunopet of malignant and normal B cells with ^{89}Zr- and ^{124}I-labeled obinutuzumab antibody fragments reveals differential CD20 internalization in vivo. *Clin Cancer Res.* 2017;23:7242–7252.
25. Morais M, Ma MT. Site-specific chelator-antibody conjugation for PET and SPECT imaging with radiometals. *Drug Discov Today Technol.* 2018;30:91–104.
26. Olafsen T, Betting D, Kenanova VE, et al. Recombinant anti-CD20 antibody fragments for small-animal PET imaging of B-cell lymphomas. *J Nucl Med.* 2009;50:1500–1508.
27. Krasniqi A, D'Huyvetter M, Xavier C, et al. Theranostic radiolabeled anti-CD20 sdAb for targeted radionuclide therapy of non-Hodgkin lymphoma. *Mol Cancer Ther.* 2017;16:2828–2839.
28. Li L, Turatti F, Crow D, et al. Monodispersed DOTA-PEG-conjugated anti-TAG-72 diabody has low kidney uptake and high tumor-to-blood ratios resulting in improved ^{64}Cu PET. *J Nucl Med.* 2010;51:1139–1146.
29. van Duijnhoven SM, Rossin R, van den Bosch SM, Wheatcroft MP, Hudson PJ, Robillard MS. Diabody pretargeting with click chemistry in vivo. *J Nucl Med.* 2015;56:1422–1428.